Formation and Sustainment of a 150 kA Tokamak by Coaxial Helicity Injection

B. A. Nelson, T. R. Jarboe, D. J. Orvis, L. A. McCullough, J. Xie, C. Zhang,* and L. Zhou

University of Washington, Seattle, Washington 98195

Coaxial helicity injection is used to produce low-aspect-ratio tokamaks with toroidal currents reaching 150 kA (highest value yet attained by helicity injection current drive) and sustained over 100 kA for many resistive diffusion times, without a current drive transformer. Current drive power efficiency, assuming no anomalous helicity dissipation, is 40% that of Ohmic. These tokamaks have a rotating $n = 1$ toroidal distortion, with poloidal distortions only on the outer bad-curvature region. Equilibrium reconstruction suggests these plasmas have up to 112 kA of closed-field toroidal current, an aspect ratio $A = 1.69$, a tokamak q profile, and a hollow toroidal current profile.

The tokamak is presently the leading contender for producing controlled magnetic fusion energy. To make an attractive reactor, some method of current drive must be utilized. When scaled to a reactor, the presently studied current drive methods, e.g., rf, neutral beam injection, and spheromak injection, have efficiencies on the order of $10^{-3} - 10^{-2}$, requiring a high recirculating power fraction [1–3]. Coaxial helicity injection (CHI) [4] offers a method of steady-state current drive that has predicted reactor efficiencies in the tens of percent. This improvement of over a factor of a hundred changes the current drive costs in a reactor from being dominant to insignificant.

Magnetic helicity is defined by $K \equiv \int \mathbf{A} \cdot \mathbf{B} \, d\tau$, where $\mathbf{A}$ is the magnetic vector potential, $\mathbf{B}$ is the magnetic flux density, and the integral is over a volume within a flux surface. Helicity is easily shown to be proportional to the arithmetic product of linked flux [5]. Plasmas described by ideal magnetohydrodynamics have fixed flux linkage topology which fixes K. In the presence of finite resistivity, K decays on resistive diffusion time scales, but the magnetic energy can decay on the much faster relaxation time scales. On these short time scales, fluctuations dissipate the magnetic energy while keeping the the global helicity constant, relaxing the plasma toward the Taylor minimum energy state [6] where the force-free equilibrium is given by $\nabla \times \mathbf{B} = \lambda \mathbf{B}$, where $\lambda = \mu_0 J/B$ is a global constant. ($J = |\mathbf{J}|$ is the current density and μ_0 is the permeability of free space.) Other effects such as nonuniform resistivity, helicity injection, and finite pressure gradients drive the plasma away from the Taylor state, with the plasma reaching a nonuniform λ equilibrium where these effects and relaxation balance. This Taylor minimum energy principle very successfully explains the equilibria and profiles of reverse field pinches and spheromaks [6].

In a tokamak, helicity is proportional to the product of toroidal and poloidal fluxes, and for a given current profile K is approximately proportional to the plasma current, I_p. Helicity "injection" can sustain I_p by applying

a bias voltage, V_{inj}, to the magnetic flux, ψ_{inj}, that penetrates two electrodes [7]. The voltage applied to the electrodes continuously injects primarily toroidal flux linking ψ_{inj}, "injecting" helicity at the rate $\dot{K}_{\text{inj}} = 2V_{\text{inj}}\psi_{\text{inj}}$ (the factor of 2 is from the injected flux linking ψ_{inj} and vice versa). Qualitatively, this can be thought of as an unstable edge-driven current producing fluctuations which flatten the J/B profile, at constant K, driving current in the interior of the plasma [8].

A tokamak using helicity injection current drive does not require the use of a transformer, allowing construction with low aspect ratio. These low-aspect-ratio tokamaks, or "spherical tori," [9] feature natural elongation, high paramagnetism, improved drift surfaces, and high predicted β limits [10]. Recent results on the low-aspect-ratio tokamak START [11] have shown robustness to tokamak disruptions for aspect ratios $A < 2$.

A power efficiency, ϵ, for helicity injection current drive relative to Ohmic can be derived for a Taylor-state tokamak and a Taylor-state injector from dissipation of energy per unit helicity arguments [12,13]. Assuming helicity balance (demonstrated for spheromaks, as yet unproved for tokamaks) yields

$$\epsilon = \frac{\lambda_{\text{tok}}}{\lambda_{\text{inj}}} = \frac{\mu_0 I_p/\Phi_T}{\mu_0 I_{\text{inj}}/\psi_{\text{inj}}} = \frac{I_p}{I_{\text{inj}}} \frac{\psi_{\text{inj}}}{\Phi_T}, \tag{1}$$

where Φ_T is the tokamak toroidal flux, and I_{inj} is the injector current. (Note this is a "true" dimensionless power efficiency, i.e., watt per watt.) The condition $\lambda_{\text{inj}} > \lambda_{\text{tok}}$ is required for helicity to flow from the injector to the tokamak; thus $\epsilon < 1$. We also note that a high injector impedance is important, as it produces a large $\dot{K}_{\text{inj}}$ (high V_{inj}) with a high efficiency (low I_{inj}). Of course, to obtain high efficiency, λ_{inj} should be nearly equal to λ_{tok}.

Electrodes used for helicity injection vary from small electron-emitting types [14] to large area coaxial types [4,15–17]. The small nonaxisymmetric electrodes have a small value of ψ_{inj}/Φ_T, and need to be heated to electron emission to produce sufficient I_{inj} for equilibrium generation. Coaxial helicity injectors have the advan-

tage of lower current density requirements, axisymmetry, and λ_{inj} similar to λ_{tok} [4], resulting in lower impurities, perturbations, and a higher efficiency, respectively. The direct incorporation of the tokamak toroidal field into the injector also gives it a high impedance [4,16].

Cowling [18] showed that axisymmetric fields cannot be sustained by axisymmetric oscillations; hence nonaxisymmetric motion is required to achieve relaxation current drive. CHI current drive experiments usually observe $n = 1$ oscillations [15–17].

The Helicity Injected Tokamak (HIT) experiment uses CHI to form and sustain low-aspect-ratio tokamaks. HIT's electrodes, shown in Fig. 1, are a 13 mm thick copper (1.25 mm W-sprayed) central column (cathode) and 10 mm thick copper (0.25 mm W-sprayed) outer conducting shells. External coils produce a predominately radial injector flux, ψ_{inj}. Hydrogen gas introduced into the injector is ionized and preheated by a 100 μF, 7 kV preionization bank (switched at $t = 0$) and a 3 mF, 1.7 kV formation bank. A 36 mF, 950 V sustainment bank then maintains the injector current. HIT diagnostics include surface magnetic field probes, a far-infrared (184.6 μm) interferometer, two 0.2 m vacuum-ultraviolet monochromators, an excluded flux loop (compensated to measure the confinement region paramagnetism $\Delta\Phi_T$), and various Rogowski loops. (The Thomson scattering system, though installed for these experiments, did not yield reliable data.) The plasma current is measured using fourteen confinement region surface probes as a "discrete" Rogowski loop, viz., $I_p \simeq \sum_{n=1}^{14} B_{p_n} \Delta\ell_n / \mu_0$, with B_{p_n} the surface poloidal field, and $\Delta\ell_n$ the appropriate distance centered on each probe. For diagnostic access, the outer shells have a 5 cm wide midplane gap held apart by 64 copper bushings called "bridges." Five toroidally spaced bridge Rogowski loops measure the current through several of these bridges. Each Rogowski loop is calibrated to the *total* current, I_b, assum-
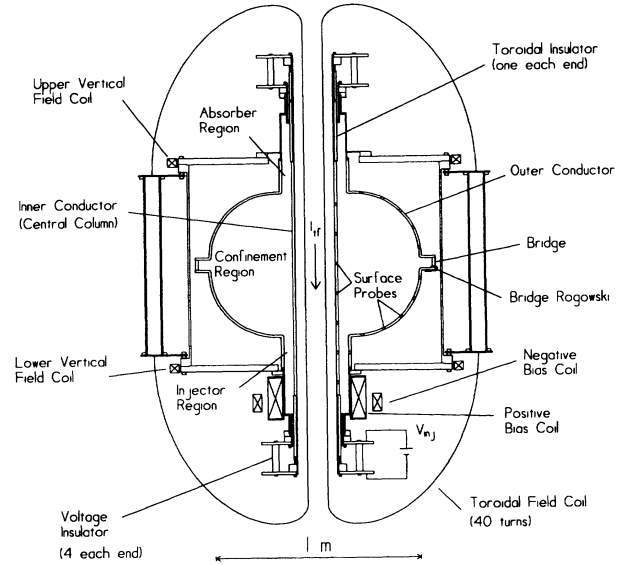

FIG. 1. A schematic layout (top view) of HIT is given, where the "injector," "confinement," and "absorber" regions are defined. The tokamak is formed and sustained between the inner and outer conductors.

ing equal current through all bridges. Thus, I_b measures the amount of I_{inj} flowing to the upper shell and the absorber region's outer conductor, with a low I_b value implying the injector current nearly encircles the closed flux region of the plasma. Wall conditioning consists of H_2 discharge cleaning followed by Ti gettering. Typical device and operating parameters are given in Table I.

A "high-current regime" of operation is reached when I_p exceeds 140 kA during the sustainment phase, shown in Fig. 2(a). This regime is characterized by a higher ratio of poloidal field on the outer wall to the inner wall, up/down symmetry, low I_b [Fig. 2(b)], and a rotating $n = 1$ toroidal distortion causing fluctuations in I_b at ap-

TABLE I. HIT parameters for a high-current regime discharge at $t = 1.0$ ms.

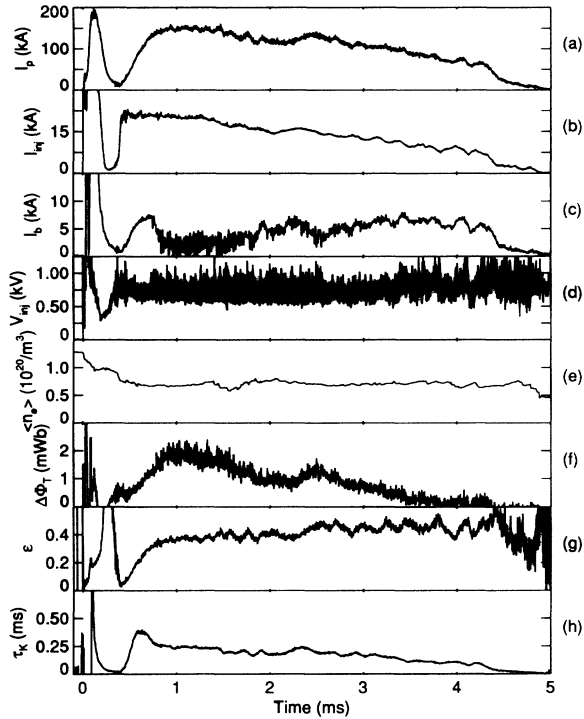| Parameter		Value		Parameter		Value	
Device				EFIT Reconstruction			
Major radius	R	0.3	m	Closed field current		112	kA
Minor radius	a	0.2	m	Open poloidal flux		2.32	mWb
Aspect ratio	A	1.5		Open field I_{pol}		3.15	kA
Magnetic field	B_0	0.46	T	Closed poloidal flux		11.5	mWb
Toroidal flux	Φ_T	100	mWb	Helicity	K	0.0017	Wb^2
Injector flux	ψ_{inj}	4.9	mWb	Axis safety factor	q_0	8.32	
				Edge safety factor	q_{95}	11.6	
Measured Parameters				Elongation	κ	1.85	
Toroidal current	I_p	150	kA	Major radius	R	0.31	m
Injector current	I_{inj}	20	kA	Minor radius	a	0.18	m
Injector voltage	V_{inj}	700	V	Aspect ratio	A	1.69	
Average density	$\langle n_e \rangle$	6×10^{19}	m^{-3}	Upper triangularity	δ_{up}	0.553	
Paramagnetism	$\Delta\Phi_T$	1.88	mWb	Lower triangularity	δ_{low}	0.913	
				Internal inductance	ℓ_i	0.26	
				Plasma volume	V	0.36	m^3

FIG. 2. Time wave forms for a high-current regime discharge: (a) plasma current I_p, (b) injector current I_{inj}, (c) bridge current I_b, (d) injector voltage V_{inj}, (e) average electron density along the chord $R = 0.24$ m $\langle n_e \rangle$, (f) paramagnetism $\Delta\Phi_T$, (g) current drive power efficiency ϵ, and (h) helicity decay time τ_K.

proximately 50 kHz (Fig. 3). The inverse growth rate of this $n = 1$ mode, $1/\gamma$, is 110 μs ($\gamma/\omega = 0.033$). Poloidal probe signals show a moving poloidal distortion at 50 kHz existing only on the outer shell probes, and approximately following the field-line pitch. The injector current, I_{inj}, is given in Fig. 2(b). (The dip in I_{inj} at $t \simeq 0.3$ ms is due to a load impedance mismatch between the preionization or formation banks and the sustainment bank.) The injector voltage, V_{inj}, shown in Fig. 2(d), has a large broadband fluctuation level in the 50–100 kHz frequency range, similar to those seen in other coaxial helicity injection experiments [12,16,17]. The electron density, n_e, averaged along a chord through $R = 0.24$ m, is $\langle n_e \rangle \sim (6 - 10) \times 10^{19}$ cm^{-3}, Fig. 2(e). The excluded flux loop shows $\Delta\Phi_T$ to be up to 2% paramagnetic, Fig. 2(f). The O VI/O V ratio increases dramatically during a discharge, saturating the O VI photomultiplier. C V is observed to increase as C VI decreases and vice versa. The current drive power efficiency, ϵ, calculated from Eq. (1), is shown in Fig. 2(g) to be approximately $\epsilon \sim 0.4$ throughout the discharge.

The EFIT equilibrium fitting code [19] is used to reconstruct the flux function ψ for this discharge, shown in Fig. 4(a) for $t = 1.0$ ms. Equilibria are calculated with no pressure gradient, $P' = 0$, and parametrized
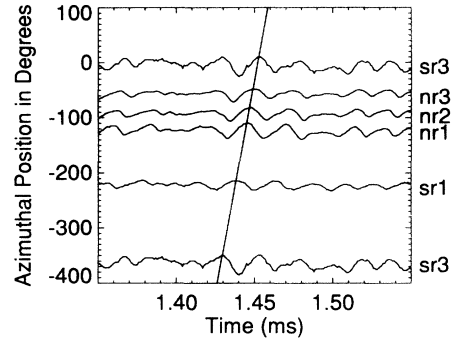

FIG. 3. The bridge Rogowski loops identify a rotating $n = 1$ distortion during high-current discharges. The vertical offset of each Rogowski loop is proportional to its toroidal position.

with separate surface functions in the confinement region, $FF' = \gamma_0 + \gamma_1 y$, and the injector region, $FF' = \beta_0$, where $F = RB_\theta$, $y = (\psi - \psi_m)/(\psi_{up} - \psi_m)$, ψ_m is the value at the magnetic axis, ψ_{up} is the value at the absorber insulator, and γ_0, γ_1, and β_0 are constants [20]. Fitting parameters consist of I_p, I_{inj}, $\Delta\Phi_T$, 15 poloidal surface probes, and 21 poloidal flux loops. Measured and calculated values agree to average errors 1.57%, 0.3%, 4.12%, 12.4%,
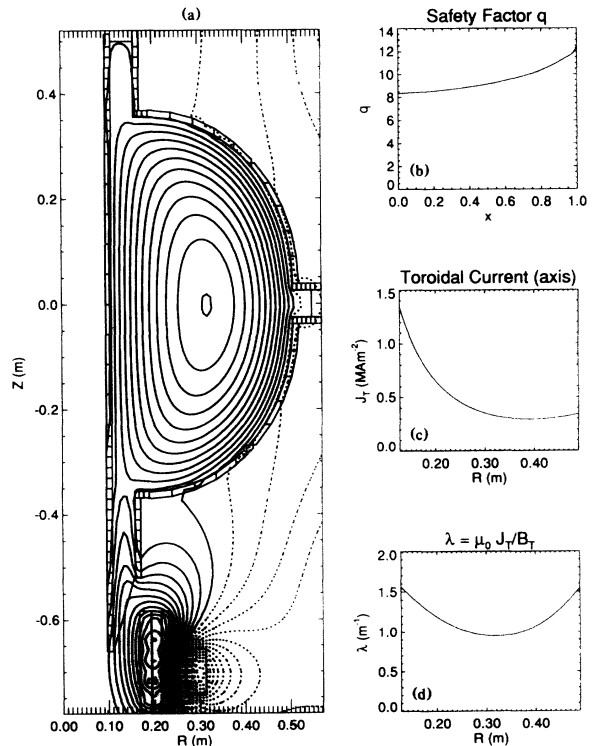

FIG. 4. EFIT reconstruction results for high-current regime discharge at $t = 1.0$ ms: (a) flux surface contours (dotted lines are $\psi < 0$), (b) q vs normalized flux x ($x = 0$ on axis, $x = 1$ at the separatrix), (c) J_T vs major radius R, and (d) $\lambda = \mu_0 J_T/B_T$ vs major radius R.

and 0.58%, respectively. Convergence of EFIT can only be reliably obtained for high-current regime discharges when I_b is low. EFIT suggests that at $t = 1.0$ ms, 2.32 mWb of the original 4.9 mWb of injector flux is pulled out and encircles the 11.5 mWb of closed poloidal flux. Approximately 3.2–4.6 kA of the 20 kA of I_{inj} flows on this open flux around the tokamak. The safety factor q, the current density J_T, and λ are given in Figs. 4(b)–4(d). Note that for this low-aspect-ratio configuration we obtain a tokamak q profile—increasing away from axis—with a *hollow* current density profile (internal inductance $\ell_i = 0.26$).

The helicity decay time τ_K is derived from helicity balance [12], yielding $\tau_K = K/(2V_{inj}\psi_{inj} - \dot{K})$, and in a tokamak is approximately equal to the plasma resistive diffusion time. K is calculated by $K = 2\int q\psi\,d\psi$ using EFIT output, integrating over the closed flux region. We then assume $K = \alpha I_p$, where $\alpha = 1.14 \times 10^{-8}$ Wb^2/A is constant with time, as verified to within 5%–10% by EFIT reconstructions for every 0.1 ms from $t = 0.6$–4.4 ms. The value of $\dot{K}$ is then obtained by numerically differentiating K. The calculated wave form of τ_K is given in Fig. 2(h), showing values in the 0.2–0.3 ms range. The entire injector voltage and flux are used to calculate τ_K, making this an average over both the injector and confinement regions. The value of τ_K in the tokamak itself is probably higher. Direct temperature measurements are not available, but spectroscopy indicates the tokamak is burning through the low Z impurities of C, N, and O. When similar conditions existed in the CTX spheromak, 100 eV electron temperatures were achieved.

The higher poloidal fields at the outer wall relative to the central column, seen only in the high-current regime, result from a larger Shafranov shift which may be due to an increase in ℓ_i or an increase in pressure. EFIT output suggests that the shift may be due to an increase in ℓ_i from a flattening of the hollow current profile. The current to the wall, I_b, may decrease because the current density on the outer flux surfaces decreases as the current at the magnetic axis increases. The $n = 1$ mode grows for several cycles indicating that it has a real and imaginary component, suggestive of a resistive mode. Thus, the data are consistent with current flattening caused by the expected double tearing mode across the separatrix [4,8]. Another interpretation is that the higher current causes a nonresonant $n = 1$ kink mode, perhaps suggesting a higher q requirement for low-aspect ratios than for high-aspect ratios. Although the high-current regime and the oscillations occur together, the causal relation is not known: The mode may be necessary to achieve high current (double tearing) or the high current itself may be causing the mode ($n = 1$ kink). In addition to these two interpretations, the fact that poloidal distor-

tions only appear in the bad-curvature region is consistent with a pressure-driven ballooning mode.

In summary, the Helicity Injected Tokamak uses coaxial helicity injection to produce low-aspect-ratio tokamaks with plasma currents reaching 150 kA and sustained over 100 kA for several milliseconds, much longer than the helicity decay time. These plasmas are characterized by a rotating $n = 1$ distortion at 50 kHz, up/down symmetry, low injector current to the upper shell, and high power efficiencies $\epsilon \sim 0.4$. Equilibrium reconstruction suggests over 112 kA of closed field toroidal current and a tokamak q profile with a hollow current profile. These experiments demonstrate coaxial helicity injection efficiently drives steady-state current in tokamaks.

* Present address: Institute of Plasma Physics, Academia Sinica, P.O. Box 1126, Hefei 230031, People's Republic of China.

[1] N. Fisch, Rev. Mod. Phys. **59**, 175 (1987).

[2] A. H. Boozer, Phys. Fluids **31**, 591 (1988).

[3] M. R. Brown and P. M. Bellan, Nucl. Fusion **32**, 1125 (1992).

[4] T. R. Jarboe, Fusion Technol. **15**, 7 (1989).

[5] H. K. Moffatt, *Magnetic Field Generation in Electrically Conducting Fluids* (Cambridge University Press, Cambridge, London, and New York, 1978).

[6] J. B. Taylor, Rev. Mod. Phys. **58**, 741 (1986).

[7] T. H. Jensen and M. S. Chu, Phys. Fluids **27**, 2881 (1984).

[8] H. P. Furth, Phys. Fluids **28**, 1595 (1985).

[9] Y.-K. M. Peng and D. J. Strickler, Nucl. Fusion **26**, 769 (1986).

[10] J. A. Holmes et al., Phys. Fluids B **1**, 358 (1989).

[11] R. J. Colchin et al., Phys. Fluids B **5**, 2481 (1993).

[12] C. W. Barnes et al., Phys. Fluids B **2**, 1871 (1990).

[13] R. Farengo and T. R. Jarboe, Fusion Technol. **20**, 407 (1991).

[14] D. S. Darrow et al., Phys. Fluids B **2**, 1415 (1990).

[15] S. O. Knox et al., Phys. Rev. Lett. **56**, 842 (1986).

[16] P. K. Browning et al., Phys. Rev. Lett. **68**, 1722 (1992).

[17] M. Nagata et al., Phys. Rev. Lett. **71**, 4342 (1993).

[18] T. G. Cowling, *Magnetohydrodynamics* (Adam Hilger, Bristol, England, 1976).

[19] L. L. Lao et al., Nucl. Fusion **25**, 1611 (1985).

[20] C. Zhang, T. R. Jarboe, and B. A. Nelson, Bull. Am. Phys. Soc. **38**, 2010 (1993).